Journal of Nuclear Materials 553 (2021) 153028

Contents lists available at ScienceDirect

Journal of Nuclear Materials

journal homepage: www.elsevier.com/locate/jnucmat

Effects of radiation damage and precipitate distribution on micro-pillar compression testing of irradiated CuCrZr

Alexandra J. Cackett[a,b,*], H.T. Vo[c], J.J.H. Lim[a], A.J. Bushby[b], P. Hosemann[c], C.D. Hardie[a]

[a] UK Atomic Energy Authority, Culham Science Centre, Oxfordshire OX14 3DB, UK
[b] School of Engineering and Materials Science, Queen Mary University of London, Mile End Road, London E1 4NS, UK
[c] Department of Nuclear Engineering, University of California-Berkeley, Berkeley, CA 94720, USA

ARTICLE INFO

Article history:
Received 3 February 2021
Revised 26 March 2021
Accepted 14 April 2021
Available online 5 May 2021

Keywords:
Size effect
Irradiation
In-situ pillar compression

ABSTRACT

The results of small-scale mechanical tests are convoluted by the so-called size effect, whereby materials appear stronger when the scale of the test is reduced to the order of microns or less. The dimensional range over which this occurs has been shown to be linked to a change in sample microstructure, such as the addition of defects induced by irradiation. To investigate this response, a CuCrZr alloy was subjected to proton irradiation and mechanically tested using micro compression of pillars with a range in size. It was found that irradiation defects dominate over the extrinsic size effect and the sensitivity to differences in precipitate microstructure was also somewhat reduced, suggesting that size-independent results could be obtained from much smaller test volumes in irradiated material compared to their non-irradiated counterparts. Finally, comparison was made between the increase in yield strength predicted by models and the experimentally measured values to establish the key parameters driving the strengthening behaviour.

1. Introduction

Small-scale mechanical testing offers a wide range of advantages when testing irradiated material. While the reduction of radioactive material volume enhances safety, extracting mechanical properties from ion beam irradiated materials enables more efficient research and development efforts [1]. There are a number of different small-scale testing techniques that have been applied to nuclear materials [1–5] with micro compression tests being a relatively recent addition to this list [6–8].

When testing materials at small-scale one has to consider the scaling effects and the fact that materials behave stronger at smaller length scales [9]. Common to all miniaturised tests is the influence of an extrinsic size effect; when the size of the test volume approaches the length scale of the material microstructure, the measured mechanical properties diverge from the bulk response [10–12]. This acts in combination with the well-established intrinsic size effect, whereby the strength of the material increases as the scale of the dominant microstructural features - e.g. grain size, precipitate spacing, dislocation density - decreases. The experimental parameters over which both these size effects act must be fully characterised if engineering-relevant data is to be extracted from small-scale tests.

Size effects in micro pillar compression experiments have been investigated for various precipitate-containing alloys. For example, Bellón *et al.* [13] performed tests in Al-Cu alloys that had either predominantly Guinier-Preston zones or θ' or θ'' precipitates. It was found that the highest strength was achieved with a fine dispersion of θ' or θ'' precipitates, which was attributed to an Orowan mechanism due to the observation of dislocation loops around precipitates in the compressed pillars. Furthermore, it was identified that extrinsic size effects were negligible when the micro-pillars (of square cross-section) had diameters $\geq$ 5 m. Alizadeh and LLorca [14] came to a similar conclusion for experiments in a Mg-4Zn alloy, which exhibited size-independent mechanical properties when the cross-section was $> 3 \times 3\mu$m. The authors additionally used an Orowan model to calculate the expected strength increase due to contributions from both precipitates and solid solution and found good agreement between the predicted values and their experimental results.

Further work has suggested that size-independent results can be obtained from even smaller samples in irradiated material compared to their non-irradiated counterpart due to a change in the dominant deformation mechanism during testing. For example, Kiener *et al.* [15] observed no extrinsic size effect in pillars with diameters as small as 400 nm in proton-irradiated Cu. This was

* Corresponding author.
E-mail address: alexandra.cackett@ukaea.uk (A.J. Cackett).

https://doi.org/10.1016/j.jnucmat.2021.153028
0022-3115/

thought to be because yield strength was dominated by the interaction between dislocations and irradiation defects. Ion-irradiated oxide dispersion strengthened (ODS) FeCr also exhibited a similar insensitivity to extrinsic size effects in pillars as small as 100 nm [16]. Decreasing the sample size required for testing irradiated material is highly desirable; any reduction in sample volume equates to a reduction in activity, and hence cost, as well as maximising the data that can be produced from limited volumes of irradiated material.

This work aims to shed light on the question of how the micro compression size effect is affected by small, hard obstacles (precipitates) in polycrystalline material and how radiation changes this response.The material selected for this study was copper-chromium-zirconium (CuCrZr). CuCrZr has been selected for use in heat-sink components of future fusion reactors such as Iter [17] since it exhibits a combination of good thermal conductivity and high strength. To better understand the changes that may occur in CuCrZr and other fusion-relevant materials, proton irradiation can be used to enable the understanding of neutron irradiation [18,19] without activating the sample. The damage implantation layer is limited to several microns, however, so testing remains restricted to small volumes. Most importantly, this materials precipitation structure can easily be tailored by specific heat treatments allowing one to change the microstructure and study the materials response with and without irradiation, allowing a unique opportunity to study the effect of specific, well-known defects on scaling laws.

As well as drawing qualitative conclusions from the results of micro-pillar compression testing of irradiated compared to non-irradiated CuCrZr, the ability of two obstacle hardening models to predict the increase in shear stress, in this case due to precipitates and irradiation defects, was also assessed. A simple dispersed barrier hardening (DBH) model developed by Seeger [20] and the Bacon Kocks Scattergood (BKS) [21] models were chosen for this comparison. These models were recently included in work by Sobie *et al.* [22], who analysed their application to irradiation-induced defects using dislocation dynamics simulations and found that such models were able to accurately predict hardening for voids and self-interstitial atom loops. It was also found that a superposition principle can be used to combine multiple predicted hardness increases due to different defect types. Bergner *et al.* [23] likewise used the DBH and BKS models to predict an increase in yield stress and found that a good fit to experimental data on neutron-irradiated Fe-Cr could be obtained. In this current work, a similar superposition principle has been used to combine hardening due to the addition of fine precipitates and radiation defects.

2. Experimental

2.1. Material

The as-received material used in this work came in the form of a solution-annealed Cu-1.0 Cr-0.06 Zr (wt%) alloy from ZOLLERN GmbH & Co. Two additional samples were produced by annealing this alloy in a vacuum furnace at temperatures of 480°C and 650 °C for two hours. Applying such heat treatments results in the generation and development of Cr-rich precipitates, the size and spacing of which varies depending on the heat-treatment temperature [24–26]. Annealing at 480 °C is known to produce the peak-aged condition, at which the material exhibits the highest strength. At 650 °C the material is over-aged and loses strength. Specimens from each of these three conditions were taken and exposed to proton irradiation, thus creating a total of six samples on which pillar compression experiments were performed.

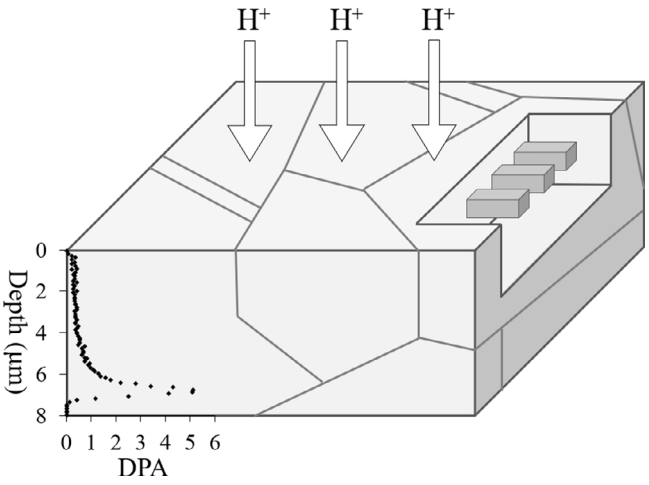

Fig. 1. Pillar orientation with respect to incident irradiation and dpa damage profile produced by SRiM.

2.2. Proton irradiation

Proton irradiation was carried out at the Dalton Cumbrian Facility, UK, using a pelletron ion accelerator [27]. All samples were irradiated using a rastered beam of energy 1 MeV and current of 25 μA, which generated a fluence of $\sim$3.37 $\times 10^{18}$ ions/cm^2 for the six-hour exposure. Samples were held in place using a tantalum mask that reduced the irradiated area to a 10 $\times$ 10 mm central region and water-cooling ensured that the bulk sample temperature did not exceed $\sim$40 °C, as measured using two thermocouples attached to the sample edge. The profile of radiation damage as a function of depth into Cu was calculated using SRiM [28] and can be seen in Fig. 1. A 5 m thick layer of approximately uniform damage of 0.4 displacements per atom (dpa) was produced, within which the pillars could be entirely contained.

2.3. Material characterisation

Characterisation of the crystal microstructure was carried out using electron backscatter diffraction (EBSD). Specimens were mechanically polished using SiC papers, followed by 1 and 0.25 m diamond suspensions, and a chemical mechanical polish using colloidal silica. EBSD was performed in a Tescan Mira3 scanning electron microscope (SEM), with grain size analysis carried out in line with ASTM standard E2627 [29].

To obtain information on average Cr precipitate size, energy-dispersive X-ray spectroscopy (EDS) was performed in a FEI Talos scanning transmission electron microscope (STEM). For this, 3 mm discs of each material condition were twin-jet electropolished using a 1:4 nitric acid to methanol mix to create a central region of electron transparency. The Super-X EDS detector was used to generate chemical maps with high spatial resolution from which precipitate size could be measured. However, since sample thickness is unknown these maps could not be used to measure precipitate spacing. Instead, precipitate spacing was calculated from data collected by electron energy loss spectroscopy (EELS) in a FEI Titan STEM. For this technique samples are required to have consistent thickness, therefore thin lamellae were prepared using the focused ion beam (FIB) lift-out method [30]. Final polishing was done using a low beam voltage of 2 kV with the sample held at 7° to the beam direction. In both cases, identification of precipitates and measurement of size and position was carried out using the Cr elemental maps and the 'Analyse particles' tool in FIJI [31].

Table 1
Values within the table represent the number of pillars tested for each combination of material condition and pillar size.

Pillar width	Non-irradiated			Irradiated		
	AR	480	650	AR	480	650
400 nm	4	4	4	4	4	4
1 m	4	4	4	4	4	4
4 m	3	3	3	3	3	3

2.4. Pillar fabrication

Samples were mechanically polished using SiC papers down to a final grade of P4000, followed by 1 and 0.25 m diamond suspensions, and a chemical mechanical polish using colloidal silica. For the irradiated sample set, this was done prior to irradiation. Using a wire saw, specimens of approximately 14 × 2.5 × 2 mm were then cut from all samples and the cut face (which was parallel to the irradiation direction) polished to remove any induced damage using the same procedure. Finally, specimens were mounted on individual pin stubs that met the requirements of the *in-situ* indenter rig.

All pillars were made using a FEI Helios 600i NanoLab dual beam SEM-FIB at the Materials Research Facility, UKAEA. Cylindrical pillars are more commonly used in micro-compression experiments, however tapering has been found to affect the stress-strain response [32] therefore for this work pillars had square cross-sections (after e.g. Kiener *et al.* [33]). Final polishing of the samples was carried out using a low beam current (80 pA) to minimise FIB damage (i.e. Ga implantation). Pillars were fabricated entirely within the first 5 m of the irradiated surface, where damage was approximately uniform at 0.4 dpa. They were orientated such that the compression direction was perpendicular to the direction of incident irradiation, and positioned along an edge so that they could be viewed from the side during compression. A schematic of this arrangement can be seen in Fig. 1.

Three sets of either three or four pillars were made in each condition, each having square cross-section and constant width to height ratio of 1:2.5 but varying widths of 400 nm, 1 m and 4 m. An experimental matrix showing the number of pillars tested for each material condition is given in Table 1.

For each material, pillars of equivalent size were all contained within single grains for each irradiated and non-irradiated condition. Not all pillar-containing grains had the same crystal orientation, therefore EBSD was used to identify the orientation and thus calculate the Schmidt factor. Maximum Schmid factor for each test was used for the purpose of normalising the results to account for different crystal orientations and enable the comparison of resolved shear stress (RSS).

2.5. In-situ pillar compression

In-situ micro compression experiments were performed using a Hysitron PI88 indenter within a FEI Quanta 3D FIB/SEM at the University of California, Berkeley, USA. The internal camera view and schematic of the indenter rig can be found in the supplementary material. A flat punch tip having a radius of 15 m was used and all tests were carried out at a constant strain rate of 0.025 s^{-1}. Pillars were compressed until a displacement of 20% of the pillar height was reached, or sooner if contact was made between the slipped pillar and surrounding material. Load and displacement data were used to calculate engineering stress, σ, and strain, ϵ, as standard,

$$\epsilon = \frac{\triangle l}{l} \tag{1}$$

$$\sigma = \frac{F}{A} \tag{2}$$

where F is the load on the indenter, A is the initial pillar cross-sectional area, Δl is the compression distance, and l is the original pillar height. There was a small degree of tapering from pillar front to back therefore the cross-sectional pillar area, A, used in the calculation of engineering stress was taken to be a trapezium,

$$A = \frac{w_1 + w_2}{2} \times d \tag{3}$$

where w_1 and w_2 are the widths as measured at the back and front of the pillar, and d is the pillar depth. Engineering stress was converted to RSS using the Schmid factor, m,

$$\sigma_R = m\sigma \tag{4}$$

3. Theory

It is well understood that plastic deformation in metals requires the movement and multiplication of dislocations. Microstructural features, such as precipitates and solute atoms, hinder this process because they act as pinning points, increasing the stress required to bend a dislocation so that it may bypass the obstacle. The distance between pinning points defines the stress increase since the strain energy of a dislocation is proportional to its line length; based on this concept, several models have been proposed that aim to predict hardening given basic microstructural parameters.

Seeger [20] proposed the following DBH model that gives the increase in shear strength, $\Delta\tau_{DBH}$, as a result of obstacles with number density N and average diameter D:

$$\Delta\tau_{DBH} = \alpha_{xDBH}\mu b\sqrt{ND} \tag{5}$$

where μ and b are the shear modulus and Burgers vector magnitude, respectively, which in this work are taken to be typical values for Cu of 45 GPa and 2.55 Å. α_{xDBH} is a strength parameter, which depends on the defect type (x). It should be noted that the use of α_{xDBH}, and the comparable fitting parameters used by the other models, can vary somewhat. Although it describes the barrier strength, it is not necessarily treated as equivalent to α as used in the Orowan equation, which depicts the character of a dislocation. The absolute values are expected to differ according to the hardening equation; values exceeding unity have been used [34] and for the DBH model it has been established that the strengthening parameter is required to vary with obstacle size to achieve a good fit to experimental data [22].

The DBH model is based on a periodic array of obstacles impeding dislocation motion, whereas the BKS model assumes a random distribution of spherical pinning points and includes an additional contribution from dislocation self-interaction. The increase in yield stress $\Delta\tau_{BKS}$ is predicted by the BKS model as follows,

$$\Delta\tau_{BKS} = \alpha_{xBKS}\frac{\mu b}{2\pi L}\left[\ln\left(\frac{L}{b}\right)\right]^{-\frac{1}{2}}\left[\ln\left(\frac{D'}{b}\right) + 0.7\right]^{\frac{3}{2}} \tag{6}$$

where the spacing between obstacles $L = \frac{1}{\sqrt{ND}}$ and D' is the harmonic average of the obstacle diameter and spacing, i.e. $D' = \frac{DL}{D+L}$. Dunn *et al.* [34] found that the BKS model was able to provide a good match with simulated data for irradiated material. They obtained fitting parameters of $\alpha_L = 1.135$ and $\alpha_\nu = 0.049$ to predict hardening due to self-interstitial (SIA) loops and voids, respectively, using fits to experimental data. They also found that these parameters were valid over a range of defect sizes (i.e. a range of total dose received during irradiation), whereas the DBH model required varying values of α as a function of defect size.

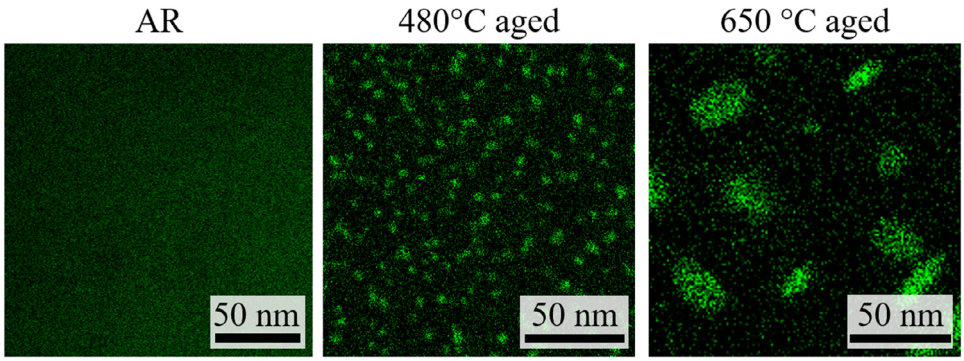

Fig. 2. EDS maps of the three non-irradiated CuCrZr samples, with green representing Cr content. (For interpretation of the references to colour in this figure legend, the reader is referred to the web version of this article.)

The as-received condition (Cr in solid solution) was taken as the "baseline" material to which the increase in strength, as calculated by Eqs. 5 and 6, was added in order to compare total shear stress. Using the characterisation methods described in Section 2.3, average values for precipitate size and spacing were obtained for the material conditions aged at 480 °C and 650 °C, which enabled the calculation of the increase in shear strength due to precipitates. The strength parameter for precipitates, α_p, was obtained by finding the best fit to experimental data for the non-irradiated material. Note that this encompassed just two data points, since only the heat-treated samples contain precipitates that contribute towards hardening.

It was not possible to perform rigorous characterisation of the irradiation defects in the irradiated samples, so to calculate the increase in shear strength due to irradiation defects values for obstacle size and spacing were instead taken from available literature. There have been several studies on CuCrZr subjected to similar irradiation conditions as this work [35–37] and it has been shown that the defects produced during irradiation in CuCrZr are very similar to that of pure Cu, being largely SFT and self-interstitial atoms (SIA) [38]. Estimates for defect size and density did not vary greatly across the literature and for this work the average values for these two parameters were taken as $N_i = 4 \times 10^{23}\ m^{-3}$ and $D_i = 2$ nm. Previous work has shown that for this alloy precipitates do not change in size or density following ion irradiation at low temperature [39], therefore the addition of radiation defects is the only microstructural change expected.

To combine the hardening contributions from precipitates, $\Delta\tau_p$, and irradiation defects, $\Delta\tau_i$, the following square superposition principle [22,40] was used,

$$\Delta\tau_T = \sqrt{\Delta\tau_p^2 + \Delta\tau_i^2} \tag{7}$$

where $\Delta\tau_T$ is the total increase in shear stress. This subsequently allowed the identification of α_i via a best fit to the irradiated data. Predicted hardening due to precipitates and irradiation defects was carried out independently for the DBH and BKS models so that the efficacy of both could be compared.

4. Results

4.1. Material characterisation

The net Cr chemical maps, produced by EDS and used for precipitate size analysis, are shown in Fig. 2. These maps clearly demonstrate the transition from Cr in solid solution for the as-received material, to Cr-rich precipitates in the peak aged material, which coarsen at a higher heat treatment temperature.

Results of the full grain size and Cr precipitate characterisation for the non-irradiated material can be seen in Table 2. Note that here the precipitate spacing refers to the average distance between precipitate edges, not distances between centre of mass. This was possible to measure since TEM lamella thickness can be calculated from the low-loss energy data produced by EELS.

Table 2
Results of Cr precipitate characterisation.

	AR	480 °C aged	650 °C aged
Grain diameter (m)	77.9	73.6	74.1
Precipitate diameter (nm)	Cr in solution	3.2 (± 1.6)	16.0 (± 7.0)
Precipitate spacing (nm)	Cr in solution	13.3	60.0

Approximately 300 precipitates, on average, were counted per condition and TEM samples were taken from the centre of grains as a Cr-depleted region of around 200 nm adjacent to grain boundaries was observed. No defined Cr segregation was observed in the as-received material, which was to be expected since the material is in a solution-annealed condition. Whilst the average grain size for each CuCrZr condition is similar, the precipitate size and spacing increases with higher heat-treatment temperature.

4.2. Micro compression experiments

Either three or four pillars of each size in each condition were tested and samples from the same set - meaning same size and material - were found to produce an extremely consistent response. An example of this can be seen in Fig. 3, which is for the 1 m pillars in the non-irradiated, as-received condition.

To compare across all sample conditions a single stress-strain curve from each type can be seen in Fig. 4. There was no considerable difference in the general deformation behaviour between irradiated and non-irradiated pillars. Strain bursts of varying magnitude were evident in most material conditions, with sudden and significant slip occurring in the irradiated, peak-aged 4 m pillars that caused the indenter tip to lose contact with the pillar as can be seen in Fig. 4(f). For the non-irradiated material, both intrinsic and extrinsic size effects influence the measured mechanical response, as expected. The 400 nm pillars exhibited the highest RSS across all material conditions and the peak-aged material (480 °C heat treatment) was the strongest when compared to pillars of the same size in as-received or over-aged material. For the irradiated sample set, however, size effects were greatly diminished. There was little influence from either sample or microstructural length scales on measured strength; only the smallest pillars showed a slight increase in RSS compared to the larger pillars but results from the three material conditions were indistinguishable.

To highlight overall trends, average values of RSS at 0.5% strain offset were identified and these can be seen in Fig. 5(a) for the non-irradiated material and Fig. 5(b) for the irradiated material. In

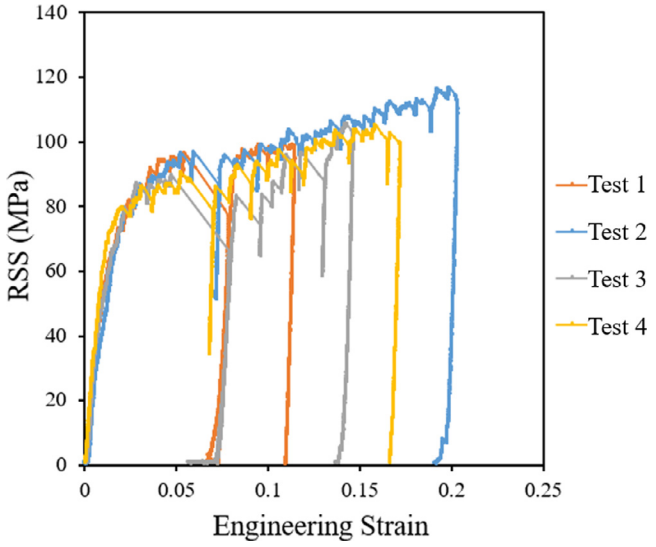

Fig. 3. Resolved shear stress (in MPa) vs engineering strain for all as-received (AR) pillars tested.

addition to the length scale effects discussed above, the irradiated data in Fig. 5 (b) also demonstrates that there was a slight increase in scatter for the tests in irradiated material. In these experiments scatter is expected in all samples since the result from each pillar inherently depends on its initial microstructure [41].

4.3. Application of hardening models

The predicted strength increase as a result of the addition of precipitates following heat treatments, as calculated using the DBH and BKS models, is shown in Fig. 6(a) alongside the experimentally-obtained average values of RSS at 0.5% strain offset. When comparing the experimental increase in strength with that predicted by the models, only data produced by the largest pillars was considered as this was the least influenced by the size effect (as evident from Fig. 5) and therefore most analogous with the models, given that the models are sample size independent. The strengthening parameters for hardening due to precipitates were identified via best fits to the non-irradiated experimental data and found to be $\alpha_{pDBH} = 0.35$ and $\alpha_{pBKS} = 0.84$. These values of α_p were able to produce very good agreement experimental data for both the peak-aged and over-aged material conditions.

The results of predicted hardening due to irradiation defects, as calculated by the two models, are shown in Fig. 6(b). The fitting parameters for the irradiation defects were $\alpha_{iBKS} = 1.34$ and $\alpha_{iDBH} = 0.48$, which were found through best fits to the experimental data. Again, a single fitting parameter for each model was able to produce good agreement with the experimental data regardless of microstructural length scale.

The four obstacle strength parameters identified are summarised in Table 3.

Table 3
Obstacle strength parameters used in the DBH and BKS models for precipitates (α_p) and radiation defects (α_i).

	DBH	BKS
α_p	0.35	0.84
α_i	0.48	1.34

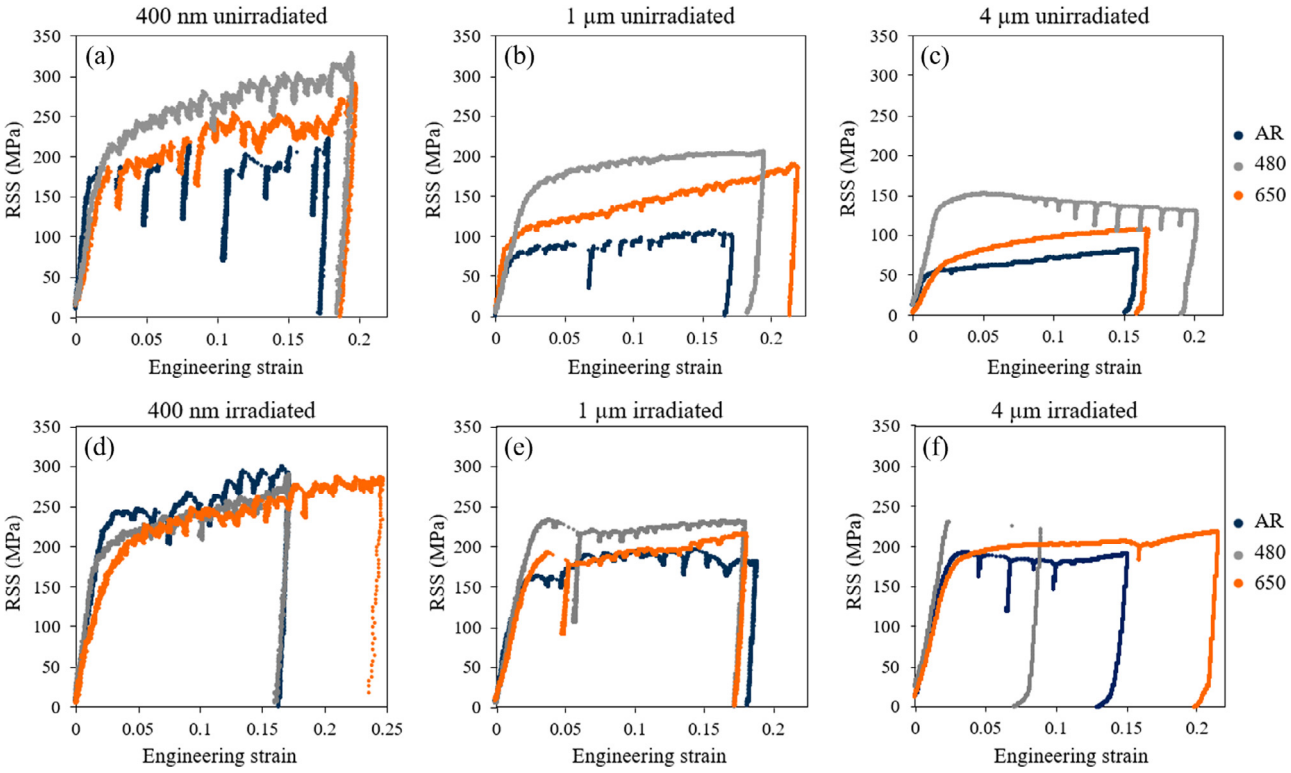

Fig. 4. Resolved shear stress (in MPa) vs. engineering strain for all samples investigated. Results are from (a) 400 nm wide, (b) 1 m wide, and (c) 4 m wide pillars at different ageing conditions in the non-irradiated material. (d) - (f) show the equivalent micro-compression data for the irradiated material.

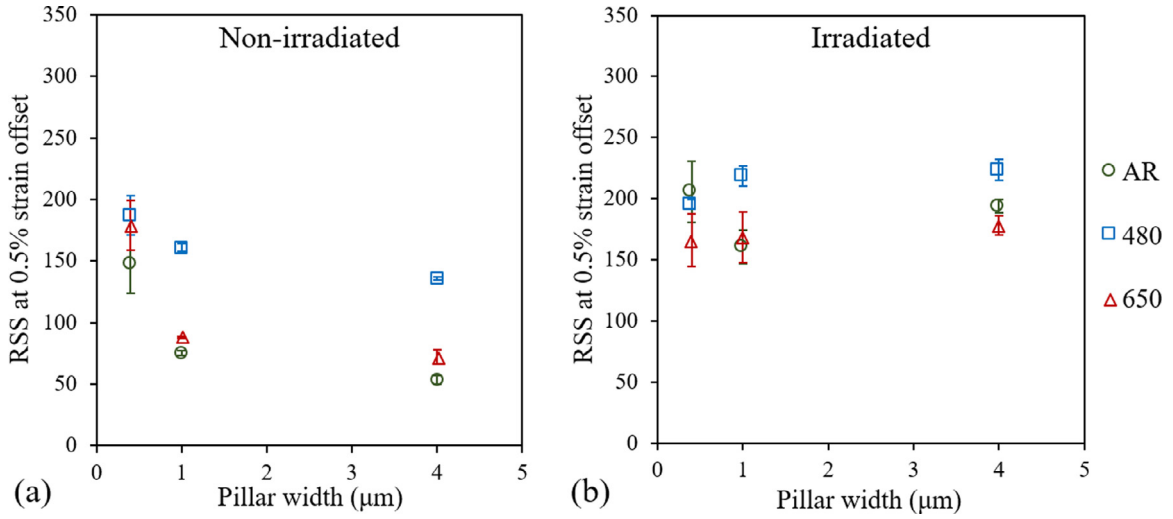

Fig. 5. Average RSS at 0.5% strain plotted against pillar size for different material ageing conditions, with error bars representing one standard deviation. Figure (a) shows the non-irradiated samples and figure (b) the irradiated samples. It is clear that the non-irradiated material experiences a size effect whereas the irradiated material does not.

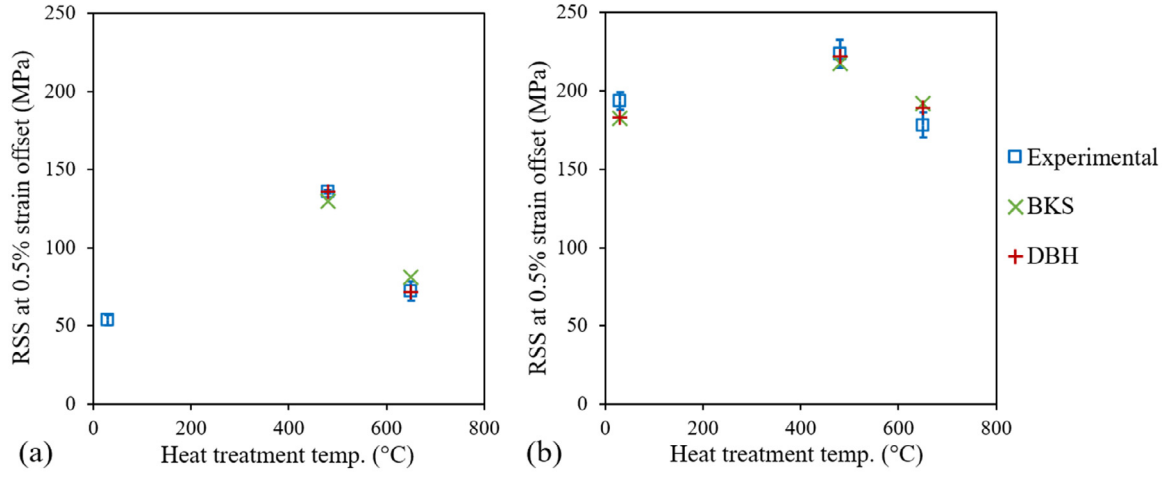

Fig. 6. Experimental (average RSS at 0.5% strain) and predicted data for (a) non-irradiated and (b) irradiated CuCrZr.

5. Discussion

In the non-irradiated alloys, strength is determined by the precipitate microstructure. The peak-aged material (480 °C heat treatment) contains the optimal size, distribution, and coherency of fine Cr-rich precipitates that oppose dislocation motion and generation thus increasing mechanical strength. Over-ageing the alloy (650 °C heat treatment) coarsens the precipitates and increases the space between them, reducing mechanical strength as dislocation lines are more easily able to bow out between pinning points. In addition to this, across all pillar sizes an extrinsic size effect, whereby smaller pillar dimensions exhibited higher strengths, was clearly observed in the micro-pillar compression experiments performed on the non-irradiated samples (see Fig. 5(a)). This type of size effect is thought to be determined by dislocation source size [42]. Plastic flow requires the generation of many dislocations and in pillars this is done via single-ended sources, since any Frank-Read sources would quickly be truncated by the pillar walls. The dislocation length, or radius of curvature for a Frank-Read source, dictates the critical stress for yield on any particular slip system therefore yield strength is proportional to the pillar width. This has been shown in 3D discrete dislocation dynamics simulations that examined strengthening mechanisms over a range of pillar sizes [43].

In contrast, for the irradiated materials there was no extrinsic size effect apparent for any of the material conditions (see Fig. 5 (b)). This was in good agreement with previous studies (e.g. [15,16]) that have shown that the presence of irradiation defects changes the extent to which the sample size effect alters mechanical response. Since defect spacing is generally orders of magnitude smaller than sample size it should be the determining factor in the effective length parameter. This can be explained by dislocation source restriction, where the effective length is the space available for dislocations to operate, which explains the diminished size effect due to sample volume in irradiated material. This is not dissimilar to work by Hou *et al.* [44] who demonstrated the absence of an indentation size effect when the grain size of polycrystalline Cu was less than six times the indentation contact area.

The obstacle strength parameters (Table 3) could be kept constant for all material conditions, despite the variation in Cr precipitate size and spacing. This suggests that it was indeed the microstructural length scales used in the DBH and BKS models that determined the predicted strength increase. For both models α_i was found to be greater than α_p, indicating that radiation defects present a more significant barrier to dislocations than precipitates. The irradiation defect parameter in particular agreed well with the values identified by similar studies. For example, Sobie *et al.*

[22] used $\alpha_{BKS} = 1.209$ and $\alpha_{DBH} = 0.435$ for SIA loops, and Dunn *et al.* [34] used $\alpha_{BKS} = 1.135$ for dislocation loops.

6. Conclusions

In this work, *in-situ* micro-pillar compression experiments were carried out on three CuCrZr conditions that had a variation in Cr-precipitate size and spacing, alongside a second set that were additionally exposed to proton irradiation. In the non-irradiated material both intrinsic and extrinsic size effects influenced the measured mechanical response. In the irradiated material, however, the pillar strengths were higher for all conditions (compared to their respective non-irradiated material equivalents) and independent of pillar size. There was also a reduced variation due to microstructure, particularly in the smallest pillars where results from the three ageing conditions are almost indistinguishable.

Provided information on characteristic microstructural length scales, two dispersed barrier hardening models were able to predict hardening due to precipitates and irradiation defects and provide a good match to experimental data. Interestingly, despite the varying form and complexity of the DBH and BKS models they were both found to produce very good agreement with experimental data for a constant irradiated microstructural parameter describing the obstacle spacing. Because the obstacle hardening models predict the strengths so well, this demonstrates that the microstructural length scales used in those models are driving the strength behaviour. This result is key, as it shows that the introduction of irradiation damage dominates over other length scales to give a size-independent strength.

The results shown here are highly promising for the nuclear materials testing community as they suggest that samples could be further miniaturised in irradiated materials whilst still generating size-independent results. Decreasing sample size continues to be an active area of research and is sought after because of the resulting reduction in activity, minimising operational risks and costs associated with handling active material. It would also maximise the number of tests that could be performed on each sample, which is vital to making best use of the limited volume of irradiated material currently being produced. Further work is needed to determine the minimum test size required for any given microstructural length scale so that bulk-scale data can be produced from such small-scale testing techniques, with the data from this systematic study providing an excellent basis for such future analyses.

Declaration of Competing Interest

The authors declare that they have no known competing financial interests or personal relationships that could have appeared to influence the work reported in this paper.

CRediT authorship contribution statement

Alexandra J. Cackett: Writing - original draft, Investigation, Formal analysis. **H.T. Vo:** Investigation, Writing - review & editing. **J.J.H. Lim:** Investigation. **A.J. Bushby:** Conceptualization, Writing - review & editing. **P. Hosemann:** Resources, Writing - review & editing. **C.D. Hardie:** Supervision, Writing - review & editing.

Acknowledgements

This work received funding via the QMUL Post-Graduate Research Fund. This work has been carried out within the framework of the EUROfusion Consortium and has received funding from the Euratom research and training programme 2014–2018 and 2019–2020 under grant agreement No 633053 and from the RCUK [grant number EP/T012250/1]. To obtain further information on the data and models underlying this paper please contact PublicationsManager@ukaea.uk. The views and opinions expressed herein do not necessarily reflect those of the European Commission. This research is being performed using funding received from the US Department of Energy Nuclear Energy University Program (DOE-NEUP) DE-NE 00008767 and the Department of Energy National Nuclear Security Administration through the Nuclear Science and Security Consortium under Award Number DE-NA0003180. The authors acknowledge the Biomolecular Nanotechnology Center (BNC) facilities at UC Berkeley.

Supplementary material

Supplementary material associated with this article can be found, in the online version, at 10.1016/j.jnucmat.2021.153028

References

[1] P. Hosemann, Small-scale mechanical testing on nuclear materials: bridging the experimental length-scale gap, Scr Mater 143 (2018) 161–168.
[2] C.D. Hardie, S.G. Roberts, A.J. Bushby, Understanding the effects of ion irradiation using nanoindentation techniques, J. Nucl. Mater. 462 (2015) 391–401, doi:10.1016/j.jnucmat.2014.11.066.
[3] D.E.J. Armstrong, C.D. Hardie, J.S.K.L. Gibson, A.J. Bushby, P.D. Edmondson, S.G. Roberts, et al., Small-scale characterisation of irradiated nuclear materials: part II nanoindentation and micro-cantilever testing of ion irradiated nuclear materials, J. Nucl. Mater. 462 (2015) 374–381, doi:10.1016/j.jnucmat.2015.01.053. http://linkinghub.elsevier.com/retrieve/pii/S0022311515000690
[4] P. Hosemann, C. Shin, D. Kiener, Small scale mechanical testing of irradiated materials, J Mater Res 30 (9) (2015) 1231–1245, doi:10.1557/jmr.2015.26.
[5] A. Reichardt, A. Lupinacci, D. Frazer, N. Bailey, H. Vo, C. Howard, Z. Jiao, A.M. Minor, P. Chou, P. Hosemann, Nanoindentation and in situ microcompression in different dose regimes of proton beam irradiated 304 SS, J. Nucl. Mater. 486 (2017) 323–331, doi:10.1016/j.jnucmat.2017.01.036. http://www.sciencedirect.com/science/article/pii/S0022311516310868
[6] E.M. Grieveson, D.E.J. Armstrong, S. Xu, S.G. Roberts, Compression of self-ion implanted iron micropillars, J. Nucl. Mater. (2012), doi:10.1016/j.jnucmat.2012.06.014.
[7] Y. Cui, G. Po, N. Ghoniem, Does irradiation enhance or inhibit strain bursts at the submicron scale? Acta Mater 132 (2017) 285–297, doi:10.1016/j.actamat.2017.04.055. http://www.sciencedirect.com/science/article/pii/S1359645417303476
[8] E. Paccou, B. Tanguy, M. Legros, Micropillar compression study of fe-irradiated 304l steel, Scr Mater 172 (2019) 56–60, doi:10.1016/j.scriptamat.2019.07.007. http://www.sciencedirect.com/science/article/pii/S1359646219304051
[9] J.W. Hutchinson, Plasticity at the micron scale, Int J Solids Struct 37 (2000) 225–238, doi:10.1016/s0020-7683(99)00090-6.
[10] S.S. Brenner, Tensile strength of whiskers, J Appl Phys (1956), doi:10.1063/1.1722294.
[11] W.D. Nix, H.J. Gao, Indentation size effects in crystalline materials: alaw for strain gradient plasticity, J Mech Phys Solids 46 (3) (1998) 411–425, doi:10.1016/s0022-5096(97)00086-0.
[12] M.D. Uchic, D.M. Dimiduk, J.N. Florando, W.D. Nix, et al., Sample dimensions influence strength and crystal plasticity, Science 305 (5686) (2004) 986–989.
[13] B. Bellón, S. Haouala, J. LLorca, et al., An analysis of the influence of the precipitate type on the mechanical behavior of al - Cu alloys by means of micropillar compression tests, Acta Mater 194 (2020) 207–223 arXiv:2005.07426, doi:10.1016/j.actamat.2020.05.040.
[14] R. Alizadeh, J. LLorca, Interactions between basal dislocations and β_1' precipitates in mg-4Zn alloy: mechanisms and strengthening, Acta Mater 186 (2020) 475–486, doi:10.1016/j.actamat.2020.01.028.
[15] D. Kiener, P. Hosemann, S.A. Maloy, A.M. Minor, et al., In situ nanocompression testing of irradiated copper, Nat Mater 10 (8) (2011) 608–613, doi:10.1038/nmat3055.
[16] D.L. Krumwiede, T. Yamamoto, T.A. Saleh, S.A. Maloy, G.R. Odette, P. Hosemann, et al., Direct comparison of nanoindentation and tensile test results on reactor-irradiated materials, J. Nucl. Mater. 504 (2018) 135–143, doi:10.1016/j.jnucmat.2018.03.021.
[17] T. Hirai, V. Barabash, F. Escourbiac, A. Fedosov, L. Ferrand, S. Gicquel, T. Jokinen, V. Komarov, A. Martin, M. Merola, Design and integration of ITER divertor components, in: Advances in Science and Technology, volume 73, Trans Tech Publ, 2010, pp. 1–10.
[18] D.J. Mazey, Fundamental aspects of high-energy ion-beam simulation techniques and their relevance to fusion materials studies, J. Nucl. Mater. 174 (2–3) (1990) 196–209, doi:10.1016/0022-3115(90)90234-E.
[19] G.S. Was, Fundamentals of Radiation Materials Science: Metals and alloys, Springer, 2016.
[20] A. Seeger, U. Essmann, Radiation damage in solids, in: IAEA, Vienna, 1, 1962, p. 101.
[21] D.J. Bacon, U.F. Kocks, R.O. Scattergood, The effect of dislocation self-interaction on the orowan stress, The Philosophical Magazine: A Journal of Theoreti-

cal Experimental and Applied Physics 28 (6) (1973) 1241–1263, doi:10.1080/14786437308227997.
[22] C. Sobie, N. Bertin, L. Capolungo, Analysis of obstacle hardening models using dislocation dynamics: application to irradiation-induced defects, Metallurgical and Materials Transactions A 46 (8) (2015) 3761–3772.
[23] F. Bergner, C. Pareige, M. Hernández-Mayoral, L. Malerba, C. Heintze, Application of a three-feature dispersed-barrier hardening model to neutron-irradiated Fe–Cr model alloys, J. Nucl. Mater. 448 (1–3) (2014) 96–102.
[24] A. Chbihi, X. Sauvage, D. Blavette, Atomic scale investigation of Cr precipitation in copper, Acta Mater 60 (11) (2012) 4575–4585, doi:10.1016/j.actamat.2012.01.038.
[25] D.J. Edwards, B.N. Singh, S. Tähtinen, Effect of heat treatments on precipitate microstructure and mechanical properties of a CuCrZr alloy, J. Nucl. Mater. 367–370 B (2007) 904–909, doi:10.1016/j.jnucmat.2007.03.064.
[26] A.J. Cackett, J.J.H. Lim, P. Klupś, A.J. Bushby, C.D. Hardie, et al., Using spherical indentation to measure the strength of copper-chromium-zirconium, J. Nucl. Mater. (2018) 5–11, doi:10.1016/j.jnucmat.2018.04.012.
[27] P.T. Wady, A. Draude, S.M. Shubeita, A. Smith, N. Mason, S. Pimblott, E. Jimenez-Melero, et al., Accelerated radiation damage test facility using a 5 MV tandem ion accelerator, Nuclear Instruments and Methods in Physics Research, Section A: Accelerators, Spectrometers, Detectors and Associated Equipment 806 (2015) 109–116, doi:10.1016/j.nima.2015.09.088.
[28] J.F. Ziegler, M.D. Ziegler, J.P. Biersack, et al., SRIM - The Stopping and range of ions in matter (2010), Nucl. Inst. Methods Phys. Res. B 268 (11–12) (2010) 1818–1823, doi:10.1016/j.nimb.2010.02.091.
[29] ASTM E2627-13, Standard Practice for Determining Average Grain Size Using Electron Backscatter Diffraction (EBSD) in Fully Recrystallized Polycrystalline Materials, 2013,
[30] L.A. Giannuzzi, F.A. Stevie, A review of focused ion beam milling techniques for TEM specimen preparation, Micron 30 (3) (1999) 197–204.
[31] J. Schindelin, I. Arganda-Carreras, E. Frise, V. Kaynig, M. Longair, T. Pietzsch, S. Preibisch, C. Rueden, S. Saalfeld, B. Schmid, J.-Y. Tinevez, D.J. White, V. Hartenstein, K. Eliceiri, P. Tomancak, A. Cardona, Fiji: an open-source platform for biological-image analysis, Nat Meth 9 (7) (2012) 676–682, doi:10.1038/nmeth.2019. http://www.nature.com/nmeth/journal/v9/n7/abs/nmeth.2019.html#supplementary-information
[32] J. Hütsch, E.T. Lilleodden, The influence of focused-ion beam preparation technique on microcompression investigations: lathe vs. annular milling, Scr Mater 77 (2014) 49–51, doi:10.1016/j.scriptamat.2014.01.016. http://www.sciencedirect.com/science/article/pii/S1359646214000207
[33] D. Kiener, C. Motz, G. Dehm, Micro-compression testing: a critical discussion of experimental constraints, Materials Science and Engineering: A 505 (1–2) (2009) 79–87.
[34] A. Dunn, R. Dingreville, L. Capolungo, Multi-scale simulation of radiation damage accumulation and subsequent hardening in neutron-irradiated α-fe, Modell. Simul. Mater. Sci. Eng. 24 (1) (2015) 015005, doi:10.1088/0965-0393/24/1/015005.
[35] D.J. Edwards, B.N. Singh, Q. Xu, P. Toft, Post-irradiation annealing of neutron irradiated cucrzr, J. Nucl. Mater. 307–311 (2002) 439–443, doi:10.1016/S0022-3115(02)01037-1.
[36] S.A. Fabritsiev, A.S. Pokrovsky, Effect of irradiation temperature on microstructure, radiation hardening and embrittlement of pure copper and copper-based alloy, J. Nucl. Mater. 367–370 (2007) 977–983, doi:10.1016/j.jnucmat.2007.03.056. Proceedings of the Twelfth International Conference on Fusion Reactor Materials (ICFRM-12), http://www.sciencedirect.com/science/article/pii/S0022311507005211
[37] M. Li, S.J. Zinkle, Physical and mechanical properties of copper and copper alloys, Comprehensive Nuclear Materials 4 (2012) 667–690, doi:10.1016/B978-0-08-056033-5.00122-1.
[38] B.N. Singh, D.J. Edwards, A. Horsewell, P. Toft, Dose dependence of microstructural evolution and mechanical properties of neutron irradiated copper and copper alloys, Technical Report, Risø National Lab., 1995.
[39] C.D. Hardie, A.J. London, J.J.H. Lim, R. Bamber, T. Tadić, M. Vukšić, S. Fazinić, et al., Exploitation of thermal gradients for investigation of irradiation temperature effects with charged particles, Sci. Rep. 9 (1) (2019) 13541, doi:10.1038/s41598-019-49585-0.
[40] U. Lagerpusch, V. Mohles, D. Baither, B. Anczykowski, E. Nembach, Double strengthening of copper by dissolved gold-atoms and by incoherent sio2-particles: how do the two strengthening contributions superimpose? Acta Mater 48 (14) (2000) 3647–3656.
[41] P.S. Phani, K.E. Johanns, E.P. George, G.M. Pharr, A simple stochastic model for yielding in specimens with limited number of dislocations, Acta Mater 61 (7) (2013) 2489–2499.
[42] T.A. Parthasarathy, S.I. Rao, D.M. Dimiduk, M.D. Uchic, D.R. Trinkle, et al., Contribution to size effect of yield strength from the stochastics of dislocation source lengths in finite samples, Scr Mater 56 (4) (2007) 313–316, doi:10.1016/j.scriptamat.2006.09.016.
[43] J.A. El-Awady, Unravelling the physics of size-dependent dislocation-mediated plasticity, Nat Commun 6 (May 2014) (2015) 5926, doi:10.1038/ncomms6926.
[44] X.D. Hou, A.J. Bushby, N.M. Jennett, et al., Study of the interaction between the indentation size effect and hall–petch effect with spherical indenters on annealed polycrystalline copper, J Phys D Appl Phys 41 (7) (2008) 074006, doi:10.1088/0022-3727/41/7/074006.